Title
Volumetric Fusion of Graphite-Doped Nylon 12 Powder with Radio Frequency Radiation

Abstract

Purpose

Additive manufacturing (AM) of thermoplastic polymers for powder bed fusion processes typically requires each layer to be fused before the next can be deposited. A volumetric fusion method such as deeply penetrating radio frequency (RF) radiation has the potential to improve the speed of the process and the mechanical properties of the polymer parts.

Design/methodology/approach

The focus of this work was to demonstrate volumetric fusion of composite mixtures containing polyamide (nylon) 12 and graphite powders using RF radiation as the sole energy source to establish the feasibility of a volumetric AM process for thermoplastic polymers. Impedance spectroscopy was used to measure the dielectric properties of the mixtures as a function of increasing graphite content and identify the percolation limit. The mixtures were then tested in a parallel plate electrode chamber connected to an RF generator to measure the heating effectiveness of different graphite concentrations. During the experiments, the surface temperature of the doped mixtures was monitored.

Findings

Nylon 12 mixtures containing between 10 and 60% graphite by weight were created, and the loss tangent reached a maximum at 35%. Selective RF heating was shown through the formation of fused composite parts within the powder beds.

Originality

The feasibility of a novel volumetric AM process for thermoplastic polymers was demonstrated in this work, in which RF radiation was used to achieve fusion in graphite-doped nylon powders.

Keywords

Additive Manufacturing; Powder Bed Fusion; Volumetric; Radio Frequency Heating; Conductive Polymer Composites; Impedance Spectroscopy

1. Introduction

The state of the art in thermoplastic additive manufacturing (AM) consists of depositing material or energy on a layer-by-layer basis, but this layer-by-layer process negatively impacts the mechanical performance of printed parts and the efficiency of fabricating them (Ajoku *et al.*, 2006; Cooke *et al.*, 2011; Gibson and Shi, 1997; Goodridge *et al.*, 2012). In the case of selective laser sintering (SLS), polymer powders are fused by scanning a laser across the powder surface. In recent years, there has been a push towards utilizing other energy sources to reduce the processing time in powder bed fusion. For example, the multi jet fusion (MJF) process was developed to reduce build times by selectively depositing thermally activated dopants to define the part geometry and fusing an entire cross-section of polymer powder with an infrared lamp (Xu *et al.*, 2019)(Hopkinson and Erasenthiran, 2004). Like SLS, however, MJF systems require each layer to be fused before the next layer can be deposited, which can contribute to lengthy build times, stair-stepping of non-horizontal surfaces, inhomogeneous shrinkage, and the development of internal residual stresses within the parts (Shen *et al.*, 2000)(Manetsberger *et al.*, 2001)(Gibson and Shi, 1997).

Volumetric AM aims to address these limitations by building a part in three dimensions rather than as a collection of two-dimensional layers. One of the first volumetric AM methods was demonstrated by projecting holographic light fields onto photosensitive resins, but the process was limited to thermoset polymers (Shusteff *et al.*, 2017). For thermoplastics, selective inhibition sintering (SIS) is the closest approximation to volumetric fusion where the part region and powder bed are separated by an inhibitor, and the entire powder surface is irradiated with an infrared lamp (Asiabanpour *et al.*, 2006). However, SIS relies on thermal conduction through the powder bed which can negatively impact the build time. Therefore, an opportunity exists for a faster energy delivery mechanism in powder-based additive manufacturing. The objective of this work is to explore the feasibility of a volumetric fusion process for thermoplastic polymers using RF radiation, thereby enabling more rapid fabrication of parts with potential improvements in mechanical properties.

Radio frequency (RF) radiation is a volumetric energy source used widely in the twentieth century for food preservation (Cathcart *et al.*, 1947), thawing (Cathcart and Parker, 1946), and therapeutic applications (Kovacs, 1945). RF heating refers to the process by which materials are subjected to an alternating electric field, and losses within the materials generate heat (Sun *et al.*, 2016). The frequency of the alternating electric field (***E***) and associated wavelength determines the penetration depth of the radiation into a medium. Frequencies below 100 MHz are generally considered RF while microwave frequencies exist at 500 MHz and above (Metaxas and Meredith, 1983). The lower frequency RF radiation is capable of deeper penetration depths and greater heating uniformity than microwaves, owing to the longer wavelength (Altemimi *et al.*, 2019). In practice, RF heating is achieved by placing a lossy material in an applicator consisting of at least two electrodes, and parallel plate electrodes are often used owing to an essentially uniform **E**-field.

The electrodes are charged with an alternating voltage input to create a time-varying **E**-field between them. Although most polymers are electrical insulators, their electrical properties can be modified through the addition of conductive dopants (Zhang *et al.*, 2007). This work aims to combine a polymer and dopant such that the effective electrical properties of the composite are suitable for RF heating and volumetric fusion of the polymer.

Additives have commonly been used to enhance the properties of the polymer in powder-based AM applications. Efforts to improve the mechanical strength of the sintered parts have included the addition of silicon carbide (Gill and Hon, 2004), clay (Jain *et al.*, 2010), glass beads (Negi *et al.*, 2015), mineral fibers (Turk *et al.*, 2017), and carbon fibers (Jansson and Pejryd, 2016) to the polymer powder. Additives have also been used to influence the thermal characteristics of the powder bed. Graphite powder has been shown to improve the laser absorption in processing polycarbonates by SLS (Ho *et al.*, 2002). Similarly, the high speed sintering process from which MJF was adapted relies on the increased infrared radiation absorption of carbon black to achieve selective fusion in the powder bed (Hopkinson and Erasenthiran, 2004). However, the use of additives to modify the RF absorption capabilities of a polymer powder bed has not been investigated and is the subject of this work.

The proposed AM process moves beyond the current layer-based approach to polymer PBF to create 3D objects rapidly in a volumetric fashion. The proposed process consists of selectively depositing an electrically conductive dopant into a polymer powder bed at room temperature to define the geometry of the intended part. The conductive dopant is engineered to absorb microwave or RF energy selectively and deposited in a layer-wise fashion to leverage the surrounding powder bed as a support structure for overhanging features and complex structures. After the part geometry is defined by the selectively deposited dopant, the entire powder bed is

radiated with RF energy to selectively fuse only the doped regions while leaving the surrounding powder bed unaffected. The primary benefit of such a process is a reduction in build time over existing methods through the use of a single stage, volumetric heating strategy. There are several challenges associated with using RF radiation to form complex structures via selectively doped powder beds. Specifically, it is challenging to tune the dopant and RF radiation process to achieve selective, volumetric fusion in a powder bed. Furthermore, the geometry of the conductively doped part can distort the associated electric field, causing non-uniform heating and deviation from the intended sintered geometry (Uyar *et al.*, 2016). The focus of this work is to establish the feasibility of a volumetric fusion process for doped thermoplastic powder beds by demonstrating selective fusion using RF radiation as the sole energy source. The powder beds are doped by hand via patterned molds to investigate the effectiveness of the process for several different prismatic geometries. The goal of this paper is to demonstrate process viability as a foundation for future work that seeks to explore automated methods for patterning the dopant to form complex structures.

2. Methods

Heat generation and fusion characteristics of conductive polymer composites exposed to RF radiation depend on the electrical properties of the polymer and dopant as well as the effective properties of the mixture. Impedance spectroscopy is used to determine the electrical properties of mixtures with varying dopant concentrations. The property measurements inform subsequent RF heating experiments where the doped mixtures are placed in powder beds and subjected to RF radiation. The heating effectiveness of the mixtures is evaluated through in-situ thermal monitoring of the powder bed surface. By selectively doping the powder beds into different geometries, the influence of the doped geometry on the uniformity of RF heating can be investigated.

2.1 Graphite-Doped Nylon 12 Composites

Nylon 12 and graphite were identified as potential candidate materials for the polymer and dopant, respectively, based on the large difference in their electrical properties. Nylon 12 has an electrical conductivity on the order of 10^{-13} S/m and dielectric loss factor in the range of 0.03-0.09, making it nearly transparent to RF electromagnetic energy (Ohki *et al.*, 2010). The electrical conductivity of graphite powder depends on the particle morphology and the direction of measurement, but typical values are in the range of 10,000 to 50,000 S/m (Deprez and McLachlan, 1988), within an order of magnitude of common metals such as steel and titanium.

The nylon 12 and graphite were available as dry powders, and both were reasonably inexpensive and safe to process. The supplier of the nylon powder was Arkema (Colombes, Fr), and the mean particle diameter was 42 µm (Arkema, n.d.). The graphite powder was supplied by Loud Wolf (Dublin, CA, USA), and the mean particle size was 44 µm with 99.9% purity. To determine the ideal nylon/graphite composition, mixtures of varying graphite contents were created. The graphite concentration was varied between 10% and 60% graphite by weight, and the samples were hand mixed in a rigid container to evenly distribute the graphite.

2.2 Impedance Spectroscopy to Measure Dielectric Properties

Impedance spectroscopy was used to measure the electrical properties of the composite powder mixtures. In RF heating applications, the degree of heat generation is governed by the complex permittivity of the material which can be evaluated according to the material's impedance. The complex relative permittivity is comprised of two parts and is a function of frequency, ω (rad/s), and the permittivity of free space, ε_0 (F/m). The real part is called the relative permittivity (ε'_r) and is a measure of the material's ability to polarize in an electric field to store

charge. The effective electrical conductivity (σ_{eff}) includes the imaginary component (ε_r'') and is a measure of the electric field losses in the material.

$$\varepsilon = \varepsilon'_r\varepsilon_0 - j\frac{\sigma_{eff}}{\omega} = \varepsilon'_r\varepsilon_0 - j\left(\varepsilon''_r\varepsilon_0 + \frac{\sigma}{\omega}\right) \qquad \text{Eq. 1}$$

At RF frequencies, the conductivity losses, σ (translational motion of free charge), dominate the dielectric relaxation losses, ε_r'' (rotational and vibrational motion of bound charge). The impedance measurements were conducted using an HP 4194A Impedance Analyzer (Palo Alto, CA, USA) with frequency sweep capabilities. The mixtures were placed in a coaxial chamber and the impedance of the chamber and sample were measured using a frequency sweep from 40 kHz to 40 MHz. Figure 1 provides a schematic of the coaxial fixture with critical dimensions labeled. To avoid fringing field effects at the upper surface of the central electrode, the sample was partially filled only to a depth, *h*, in the chamber. Partially filling the chamber ensured a tangential **E**-field boundary condition at the surface of the mixture during the measurements.

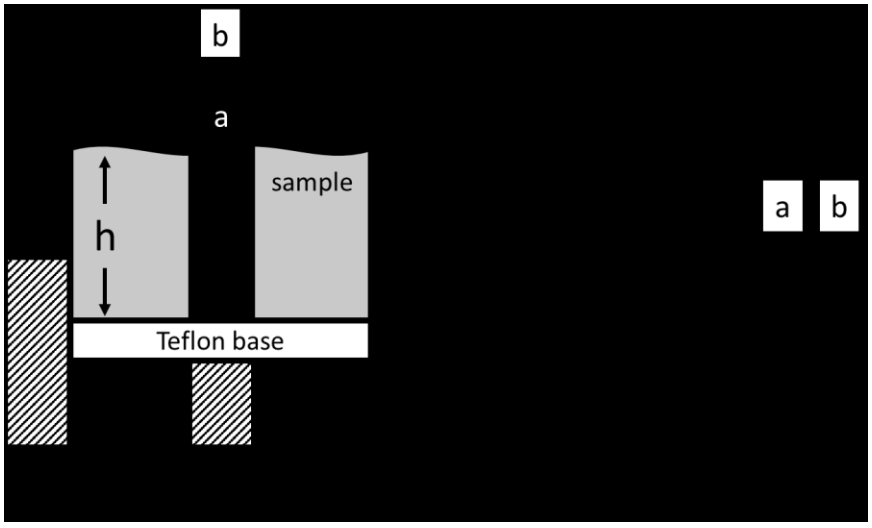

Figure 1 *Diagram of the coaxial chamber used for impedance measurement. The diameter of the inner electrode (a) was 1.59 cm, and the diameter of the outer electrode (b) was 7.94 cm. The powder was held in place by a Teflon base that separated the two electrodes. Copper strips soldered to the electrodes provided connection to the input terminals of the impedance analyzer.*

The impedance analyzer measured the total complex impedance, Z_{meas}, of the fixture and sample at each frequency:

$$Z_{meas} = R_{meas} + jX_{meas} \quad \text{Eq. 2}$$

where R_{meas} and X_{meas} are the measured resistance and reactance, respectively, and reactance is a function of angular frequency, ω, inductance, L, and capacitance, C:

$$X_L = \omega L \quad \text{Eq. 3}$$

$$X_C - \frac{1}{\omega C} \quad \text{Eq. 4}$$

To determine the properties of the sample alone, the parasitic resistance (R_{fix}), inductance (L_{fix}), and capacitance (C_{fix}) from the fixture were removed in addition to the capacitance of the air displaced by the sample within the coaxial chamber (C_{air}). Figure 2 shows an equivalent circuit of the fixture in which C_{mat} and R_{mat} are the capacitance and resistance of the material and Z_{meas} corresponds to the uncorrected, measured impedance. The characteristic resistance, inductance, and capacitance of the coaxial fixture were measured to be 3.06 Ω, 119 nH, and 5.22 pF, respectively.

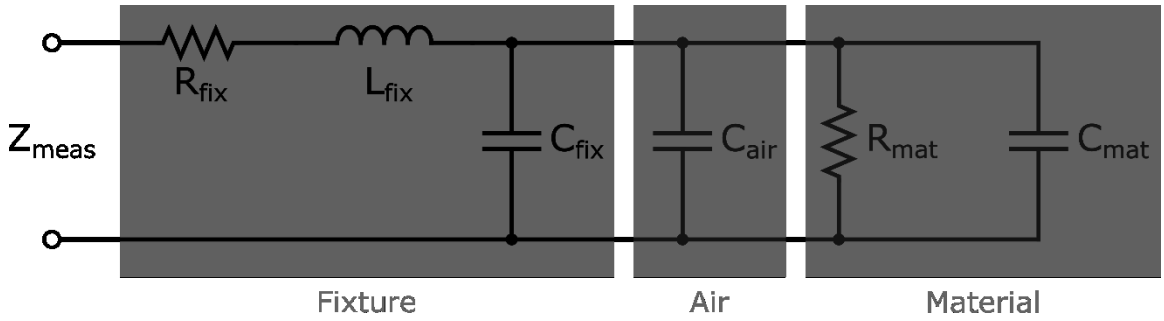

Figure 2 *Circuit diagram for the impedance measurements. The parasitic R, L, and C components of the fixture must be removed from the measured impedance to determine the complex capacitance of the material.*

The series fixture resistance and inductance were removed according to Equation 5, and the remaining quantity represents the impedance of the material and air within the chamber. The

materials do not contribute to inductive measurements owing to the absence of a physical mechanism for storing magnetic field energy.

$$Z_{mat+air} = \left(R_{meas} - R_{fix}\right) + j\left(X_{meas} - \omega L_{fix}\right) = R_{mat+air} + jX_{mat+air} \quad \text{Eq. 5}$$

Next, the impedance measurements were converted to admittance by taking the complex reciprocal. Admittance is also a complex quantity composed of the conductance (G) and susceptance (B). The conversion from impedance to admittance allows the parallel capacitance of the fixture and displaced air to be removed more readily through the susceptance.

$$Y_{air+mat} = \frac{1}{Z_{air+mat}} = G_{air+mat} + jB_{air+mat} \quad \text{Eq. 6}$$

The relative permittivity of air is approximately one, and thus the capacitance of the air displaced is represented by the geometry of the chamber with inner and outer electrode diameters, a and b, the sample depth, h, and the permittivity of free space, ε_0.

$$C_{air} = \frac{2\pi\varepsilon_0 h}{ln\left(b/a\right)} \quad \text{Eq. 7}$$

The complex admittance of the material was then determined by removing the capacitance of the fixture and displaced air from the susceptance. The conductance of the air in the fixture (G_{air}) was assumed to be negligible.

$$B = \omega C \quad \text{Eq. 8}$$

$$Y_{mat} = G_{air+mat} + j\left[B_{air+mat} - \omega\left(C_{fix} - C_{air}\right)\right] = G_{mat} + jB_{mat} \quad \text{Eq. 9}$$

With all relevant parasitic properties removed, the capacitance of the material could be determined through the susceptance and frequency.

$$C_{mat} = \frac{B_{mat}}{\omega} \quad \text{Eq. 10}$$

The effective electrical conductivity (σ_{eff}) and the relative permittivity (ε'_r) were measured from the complex capacitance as follows:

$$\sigma_{eff}(\omega) = \frac{G_{mat}(\omega) ln\left(b/a\right)}{2\pi h} \quad \text{Eq. 11}$$

$$\varepsilon'_r(\omega) = \frac{C_{mat}(\omega) ln\left(b/a\right)}{2\pi \varepsilon_0 h} \quad \text{Eq. 12}$$

Although the parallel resistance of the material does not appear directly in the conductivity calculation, it is taken into account implicitly through the conversion of impedance to admittance. It is important to note that the capacitive susceptance is a function of frequency, so the electrical properties are evaluated at a specific frequency, which is 27.12 MHz in this case.

2.3 RF Heating Apparatus

The source of the RF radiation was a 560 W short wave diathermy machine manufactured by the Burdick Corporation (Milton, WI, USA) with an operating frequency of 27.12±0.16 MHz according to the frequency bands allocated for industrial, scientific, and medical applications (Mehdizadeh, 2015). The diathermy machine featured a crystal controlled oscillator to minimize variation in the output frequency. In any RF application, maximum power transfer occurs when the load impedance matches the source impedance. The impedance was matched to the load by manually adjusting the output and tuning controls on the machine until the maximum current was achieved, indicating the system was at resonance (Maxson, 1948). Modern diathermy equipment incorporates a matching circuit to continually tune the system without intervention.

The applicator, shown in Figure 3, consisted of parallel copper plates separated with threaded Teflon rods to enable adjustment of the electrode spacing. The electrodes were connected directly to the output of the diathermy machine and enclosed in a Faraday cage to prevent RF

leakage. The electrode voltage was monitored through a differential capacitive voltage divider and an Iwatsu SS-5321 oscilloscope connected to the diathermy machine.

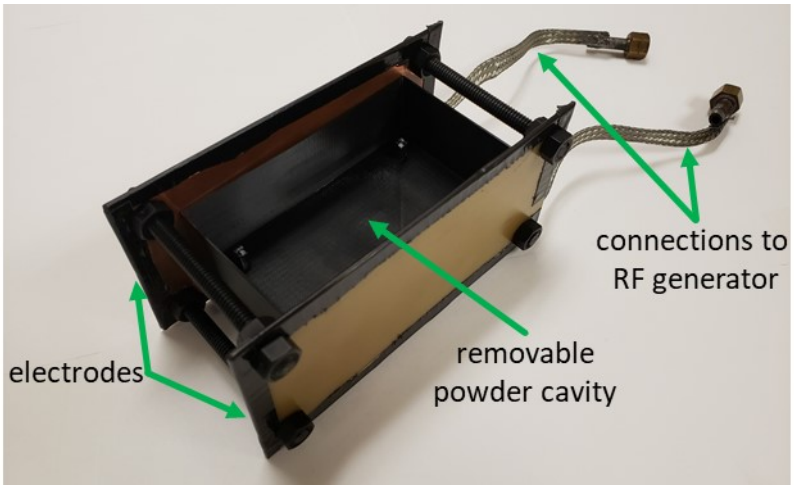

Figure 3 *Experimental applicator showing powder cavity, electrodes, and connections to RF generator*

In-situ thermal monitoring of the samples was achieved using a FLIR E60 longwave infrared camera (λ = 7.5 to 13 μm) that was mounted above the samples. The RF chamber, applicator, and camera configuration used in the experiments is shown in Figure 4. Non-contact infrared imaging was preferred over contact measurements such as thermocouples because it has no effect on the applied electric field, although it limits the measurements to the powder surface. Additionally, the IR measurements captured the temperature field, showing how the temperature was distributed across the surface.

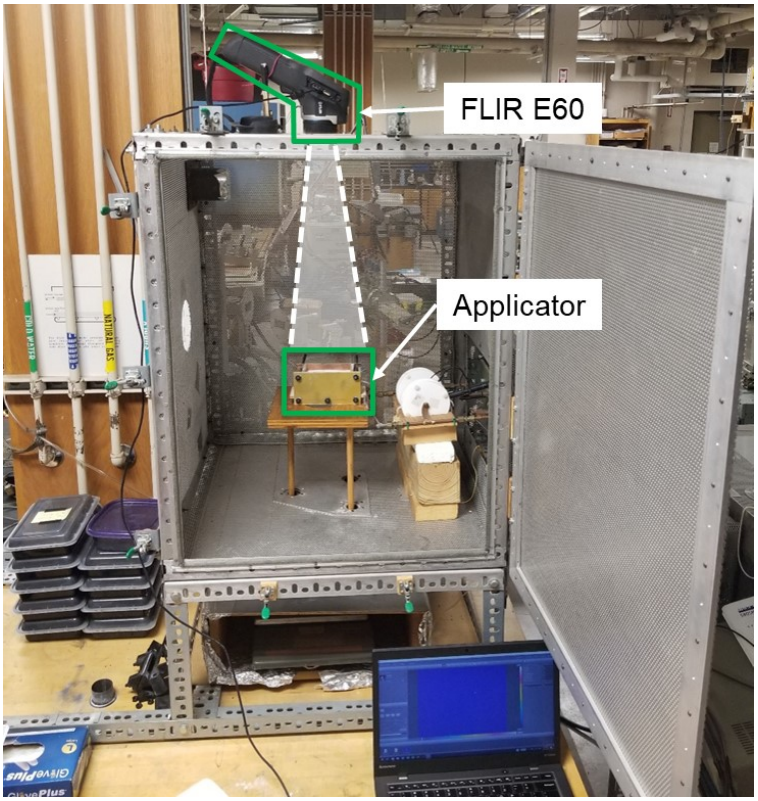

Figure 4 *Faraday cage surrounding applicator showing IR camera mounted above the sample*

2.4 Sample Preparation

The goal of the RF heating experiments was to demonstrate selective heating in a powder bed containing virgin and doped powders. As a proof of concept, the powder bed was separated into two distinct regions of virgin and doped powder. Thin PLA forms, shown in Figure 5, were used to selectively dope the powder bed into regions with circular, square, and rectangular cross sections. The forms allowed the geometry of the doped region to be clearly defined, but limited the geometry to prismatic structures. Other layer-based methods such as binder jetting could be used to pattern the dopant layer-by-layer and create parts with greater complexity, but these more complex objects are the subject of future work.

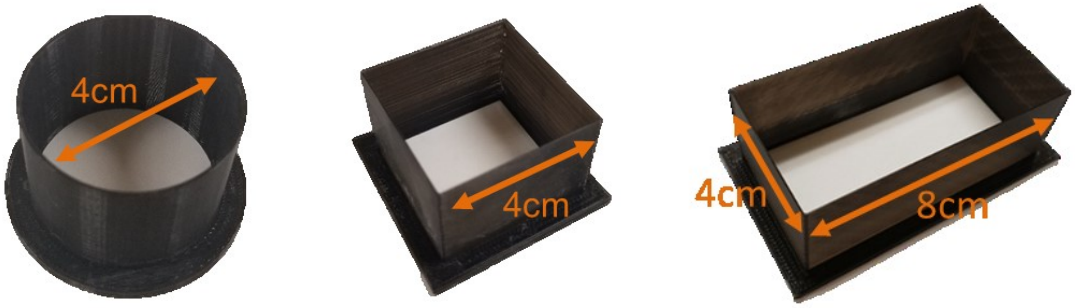

Figure 5 *Thin forms used to selectively dope the powder bed into regions of circular (left), square (center), and rectangular (right) cross sections.*

The samples were prepared according to the steps outlined in Figure 6. The chamber was first partially filled with virgin nylon power. Then, a small form was placed in the center and surrounded on all sides by additional virgin powder. Lastly, the doped powder was placed in the cavity created by the form to a depth of approximately 1 cm, and the form was removed.

Figure 6 *Process showing how the PLA forms were used to separate doped powder from virgin. a) The chamber was filled with a base layer of virgin powder. b) The form was placed in the center of the chamber and surrounded by additional powder to create a cavity. c) The cavity was filled with graphite-doped powder. d) The form was removed to create an interface between doped and virgin powder.*

After the form was removed, the powder bed consisted of a doped region with the cross section of the form surrounded by virgin powder. In this way, an unimpeded interface between the two regions was preserved to allow thermal conduction directly between them. In maintaining the boundary between the doped and virgin regions, the selectively doped powder bed provided a close approximation to the intended distribution of dopant in the powder bed as part of a volumetric RF

AM process. After defining the geometry of the doped region, the powder bed was placed between the electrodes in the RF chamber for the heating experiments.

3. Results and Discussion

3.1 Electrical Properties of Graphite-Doped Nylon 12 Mixtures

The effective electrical conductivity defined in Equation 11 represents the total loss factor of the material at a given frequency but does not provide information about the type of losses that are present. Electrical losses in time-varying fields are comprised of conductive (translational) and polarization (rotational and vibrational) components. Although the specific form of loss does not influence the RF heating characteristics of the material, identifying the loss mechanisms can explain the behavior of the nylon/graphite composites as the graphite composition is increased. The frequency response of the effective electrical conductivity at a given graphite loading can be used to distinguish the conductive (σ) losses from the losses due to polarization (ε''). Figure 7 documents the effective electrical conductivity as a function of frequency for the nylon mixture containing 30% graphite by weight.

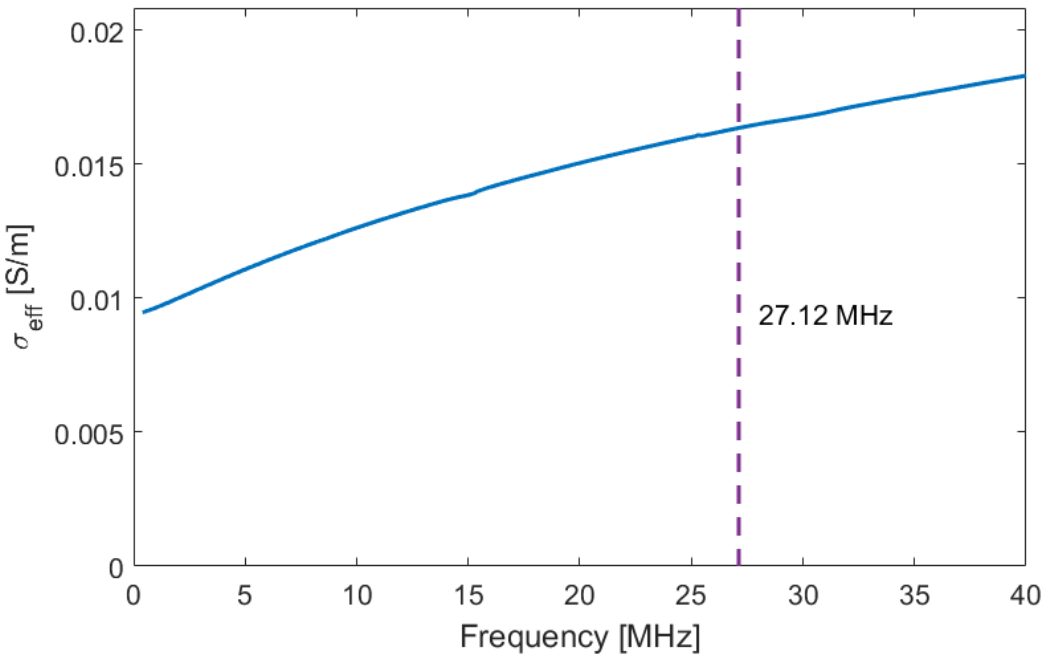

Figure 7 *Effective electrical conductivity vs. frequency for 30% graphite by weight*

The effective electrical conductivity can be expressed as a function of frequency as in Equation 13. The conductivity term (σ) is called the DC conductivity because it typically does not exhibit a frequency dependence. The effective electrical conductivity is sometimes referred to as the AC conductivity to include the frequency dependent polarization term (ε'').

$$\sigma_{eff} = 2\pi f \varepsilon_0 \varepsilon'' + \sigma \qquad \text{Eq. 13}$$

Equation 13 describes a line in which the y-intercept corresponds to the DC conductivity, and the slope is related to the polarization losses. A linear regression on the electrical conductivity data in Figure 7, then, can provide a comparative estimate of the sources of loss in the material. The linear regression on the 30% mixture data gives an R^2 correlation of 0.98 and DC conductivity of 0.0103 S/m. At the design frequency of 27.12 MHz, the total effective electrical conductivity is 0.0161 S/m. An estimate of the polarization loss can be determined by subtracting the DC conductivity (0.0103 S/m) from the total effective conductivity (0.0161 S/m) at 27.12 MHz. The relative proportion of each loss mechanism is estimated by dividing the DC conductivity and polarization

loss by the total conductivity. By this estimate, 36% of the loss is due to polarization effects while the remaining 64% can be attributed to electrical conduction.

The effective electrical conductivity as a function of frequency for mixtures containing between 10% and 60% graphite by weight is shown in Figure 8. In general, the effective electrical conductivity increases with frequency due to the combination of conductive and polarization losses. However, at graphite concentrations that are 40% by weight and higher, the conductivity decreases with increasing frequency.

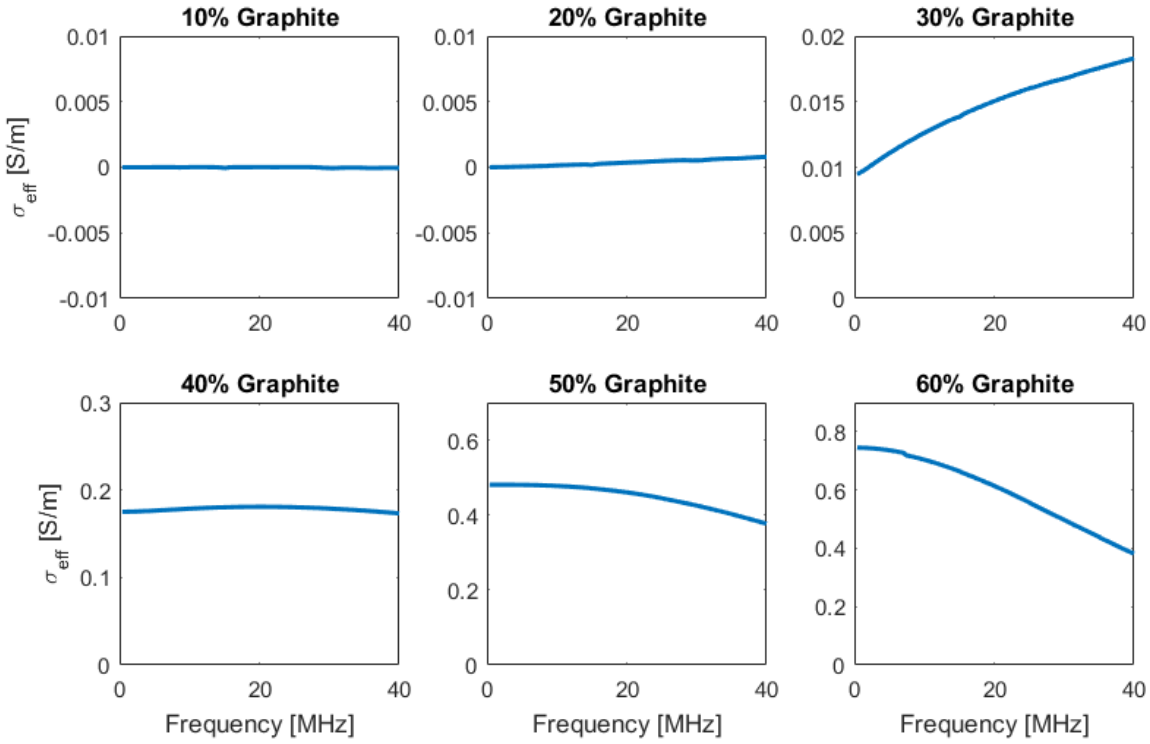

Figure 8 *Effective electrical conductivity vs. frequency for nylon/graphite mixtures containing between 10% and 60% graphite by weight.*

From the conductivity data, it appears that both polarization and conductive losses contribute to the total effective conductivity of the nylon and graphite mixtures. In filler-matrix composites, the dominant polarization loss mechanism is Maxwell-Wagner interfacial loss where free charges accumulate at the particle interfaces (Zhou *et al.*, 2017). The conduction losses in

conductive composites can also arise from interfacial effects that are similar to Maxwell-Wagner (Michael *et al.*, 1991). As the frequency is increased, the charge flux is limited by the drift velocity of the electrons within the graphite which constitutes a loss mechanism and contributes to heating. The frequency dependence of the electrical conductivity also changes with increasing graphite content, possibly owing to the formation of larger conductive networks within the mixtures.

The effective electrical conductivity at 27.12 MHz as a function of graphite content is documented in Figure 9. The measurement results suggest the percolation limit for the nylon and graphite mixtures occurs around 30% graphite by weight. Below the percolation limit, the nylon powders prevent electrical conduction through physical separation of the graphite particles (i.e. low capacitive coupling). As the graphite content is increased above 30%, a steady increase in the electrical conductivity is observed.

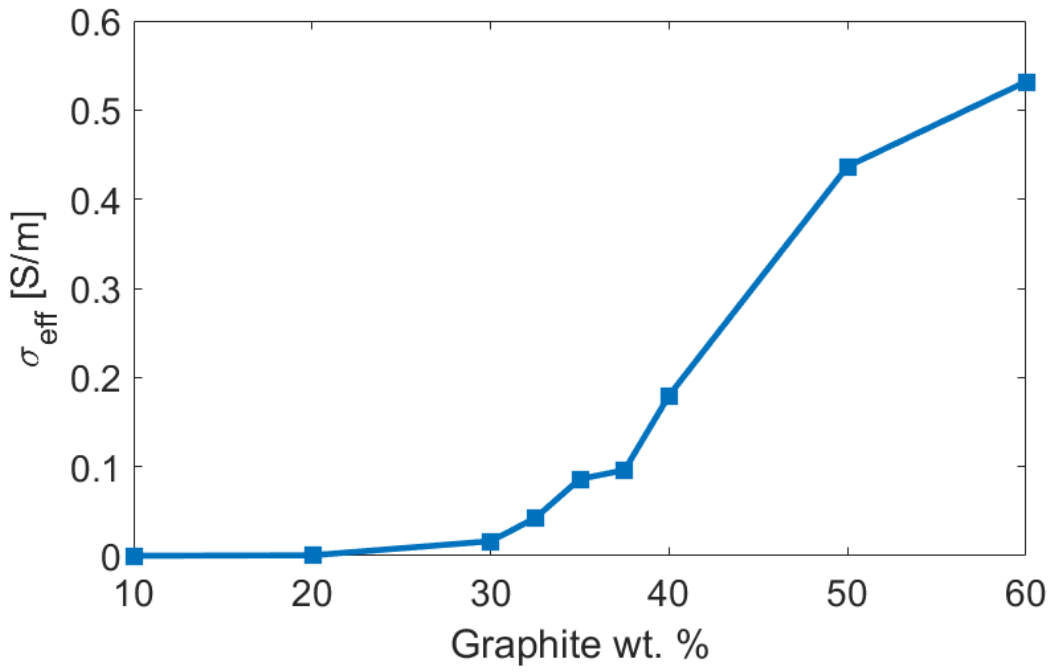

Figure 9 *Effective electrical conductivity as a function of graphite content at 27.12 MHz*

In previous studies investigating the effect of increasing carbon black content on polymer composites, the percolation limit was clearly defined by a sharp increase in the electrical

conductivity and quickly leveled out at higher concentrations (Zhang *et al.*, 2007)(Socher *et al.*, 2011). The percolation limit is not as clearly defined for the nylon/graphite mixtures, and the electrical conductivity gradually increases over a wide range of graphite content. One possible explanation for the wider percolation window in the graphite mixtures is that the anisotropic nature of graphite means the formation of conduction pathways is not a function of direct contact alone, but also the orientation of the graphite particles. In experiments conducted by Deprez et al. (Deprez and McLachlan, 1988) and Marinković et al. (Marinković *et al.*, 1971), the effect of graphite orientation on the conductivity was studied by increasing the packing pressure of graphite powders. As the packing pressure increased, the graphite particles preferentially reoriented to cause an increase in electrical conductivity. If the orientation of the graphite powders within the nylon composites is random, then it would be expected that increasing the loading would cause percolation to occur over a wider range of graphite concentrations.

In addition to the conductivity, the relative permittivity of the mixtures increases with graphite content. Shown in Figure 10, the relative permittivity appears to be divided into two distinct linear regions. The region of graphite concentrations below 37.5% is characterized by a gradual increase in the relative permittivity. Above 37.5%, however, the relative permittivity grows much more rapidly.

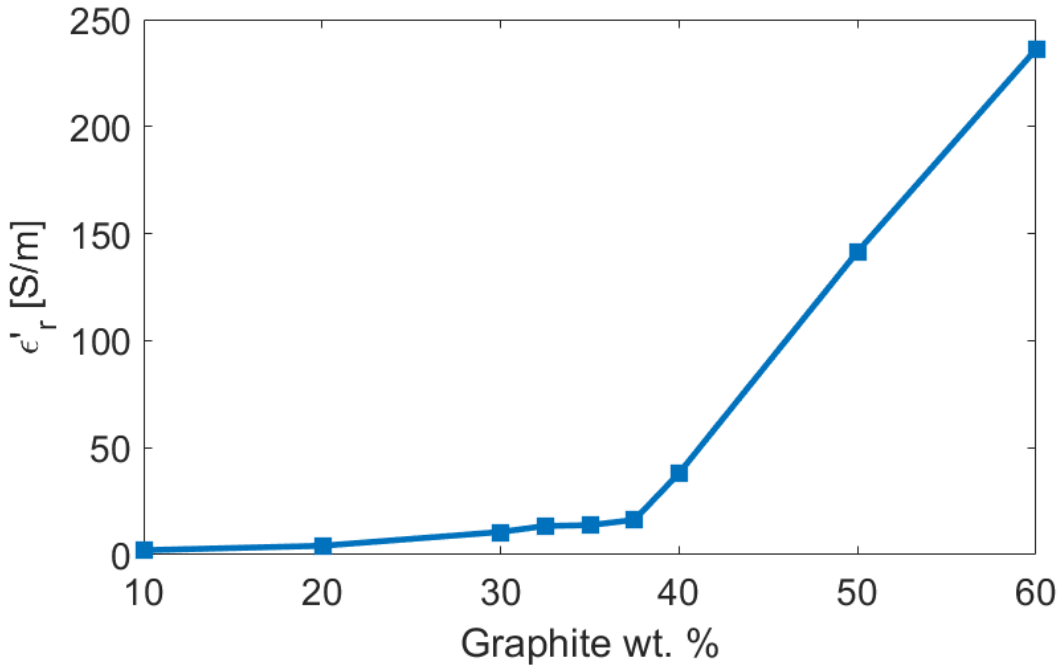

Figure 10 *Relative permittivity as a function of graphite content at 27.12 MHz*

The observed increase in relative permittivity with increasing conductive filler content agrees with previous studies. It has been shown that conductive fillers in a polymer matrix exhibit an abrupt change and faster growth near the percolation threshold (Yacubowicz and Narkis, 1986)(Dahiya *et al.*, 2007). The permittivity increase is most likely caused by charges building up at the interfaces between the conductive filler and the matrix which, interestingly, is the same mechanism that contributes to losses within the material (Wang *et al.*, 2018)(Zhou *et al.*, 2015). Even at high graphite loadings, the polymer causes small insulating gaps between the graphite particles, and the system behaves like a network of connected capacitors (Zhou *et al.*, 2017). As the graphite content is increased, the number of interfaces also increases causing a rise in the total capacitance and thus permittivity of the system.

The relative permittivity and effective conductivity both influence the RF heating characteristics of a material. The power dissipated is a function of the effective electrical conductivity as well as the electric field developed within the material (Metaxas and Meredith,

1983). Within the material, the electric field is reduced by a factor of ε'_r due to atomic polarization that creates an opposing electric field (Haus, 1989). Superposition of the induced electric field with the applied electric field causes a reduction in the power dissipation as the relative permittivity increases. Therefore, there is a tradeoff between the material's conductivity and relative permittivity in RF heating. For this reason, the loss tangent is often considered in RF heating applications. The loss tangent of a material is the ratio between the effective electrical conductivity and relative permittivity (Equation 14).

$$tan\delta = \frac{\sigma_{eff}}{\varepsilon'_r \varepsilon_0 \omega} \qquad \text{Eq. 14}$$

The loss tangent as a function of graphite content for the nylon mixtures is shown in Figure 11. Since the conductivity and relative permittivity both increase with graphite loading, the loss tangent provides a clear demonstration of the tradeoff that takes place. As the graphite content is increased, the loss tangent rises rapidly. However, it reaches a maximum value around 35% graphite before declining. The decrease in the loss tangent at higher graphite loadings shows the relative permittivity grows faster than the conductivity, and the shape of the trend aligns with the results of Yacubowicz et al. (Yacubowicz and Narkis, 1986). The loss tangent results suggest the 35% graphite mixture is expected to have the highest degree of heating in RF radiation.

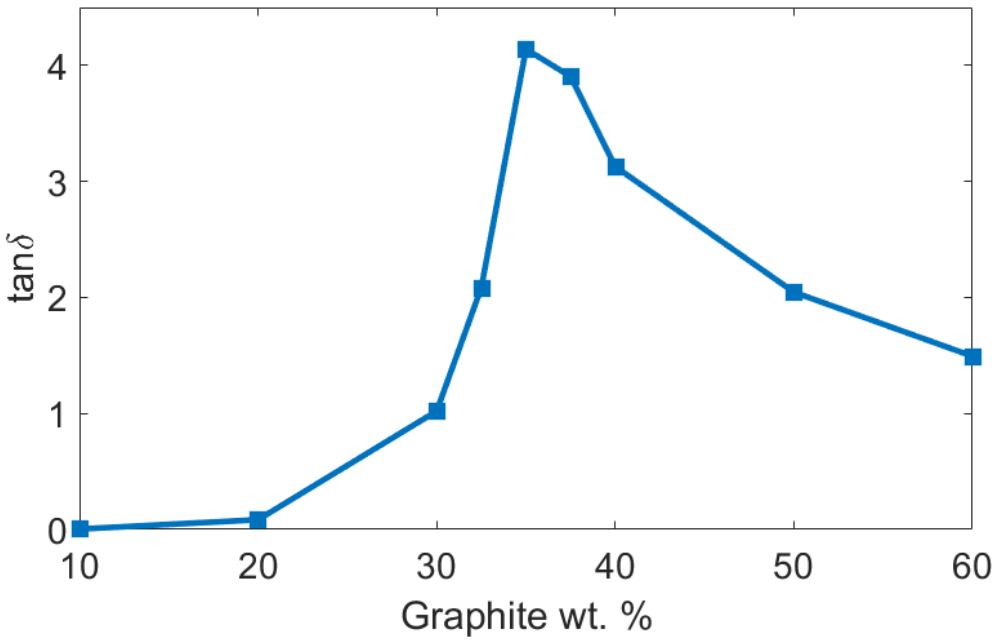

Figure 11 *Loss tangent as a function of graphite content at 27.12 MHz*

There is an inverse relationship between the electrical conductivity and penetration depth of RF radiation. The penetration depth as a function of graphite loading can be calculated from the electrical conductivity measurements, and the results are shown in Figure 12. The electrical conductivity increases with graphite content which then causes the penetration depth to decrease. The penetration depth for the 10% graphite mixture is 14.4 m and drops to 6.6 cm in the 60% sample. At 35% graphite by weight, where the loss tangent reaches a maximum, the penetration depth is 16.4 cm. Penetration depth is an important parameter in RF heating because it determines the maximum part dimensions that can be heated. The penetration depth also decreases with increasing frequency, and so the maximum part dimensions are reduced as the radiation frequency moves from RF to the microwave range (Metaxas and Meredith, 1983).

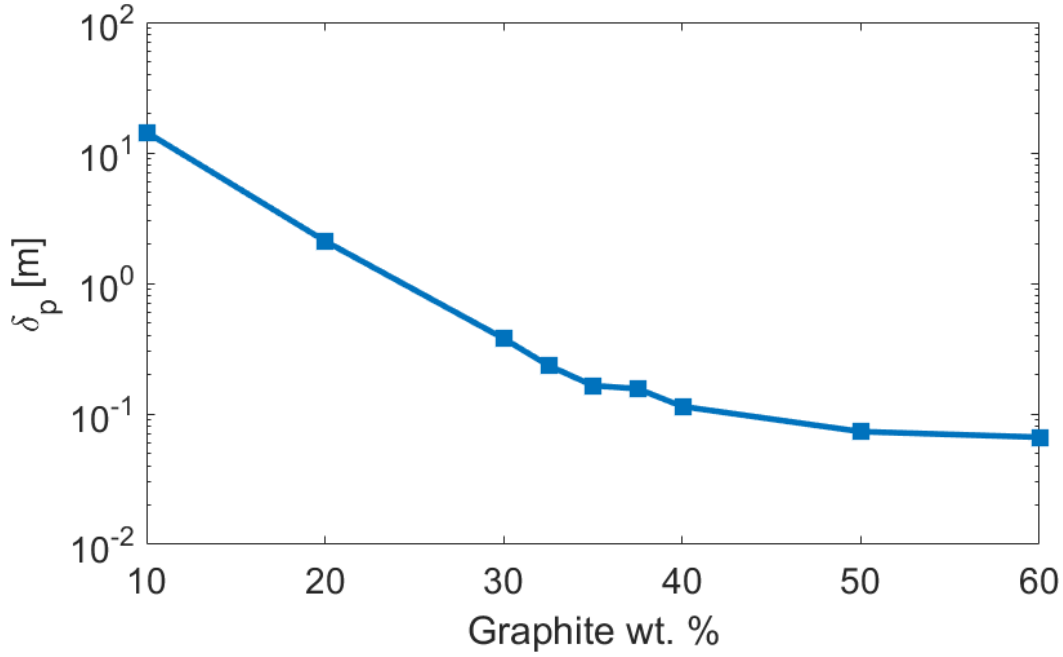

Figure 12 *Penetration depth as a function of graphite content at 27.12 MHz*

The electrical properties of the nylon/graphite mixtures reveal interesting insights into the mechanism of charge storage and loss. The tradeoff between the electrical conductivity and relative permittivity in the loss tangent results indicate the expected dopant levels for the most effective RF heating. The penetration depth gives additional support for the choice of RF over higher frequencies and establishes the upper limit on the size of parts to be heated.

3.2 RF Heating Experiments for Graphite-Doped Nylon 12 Mixtures

RF heating experiments were conducted to measure the effect of varying the graphite content on the temperature rise of the doped powders. The electrical property measurements were useful in determining the sources of charge storage and loss, but the properties represent intrinsic behavior of the materials and do not account for geometric effects. For each of the nylon/graphite mixtures, the circular form was used to define a cylindrical doped region. The circular cross section (Figure 5) was chosen for the initial experiments to minimize the number of corners and edges on the geometry that could lead to non-uniform heating. The tuning parameters of the RF generator

were held constant for all experiments, and the surface temperature of the powder bed was recorded with the infrared camera. The average surface temperature of the doped region after 90 seconds of RF exposure as a function of graphite content is documented in Figure 13.

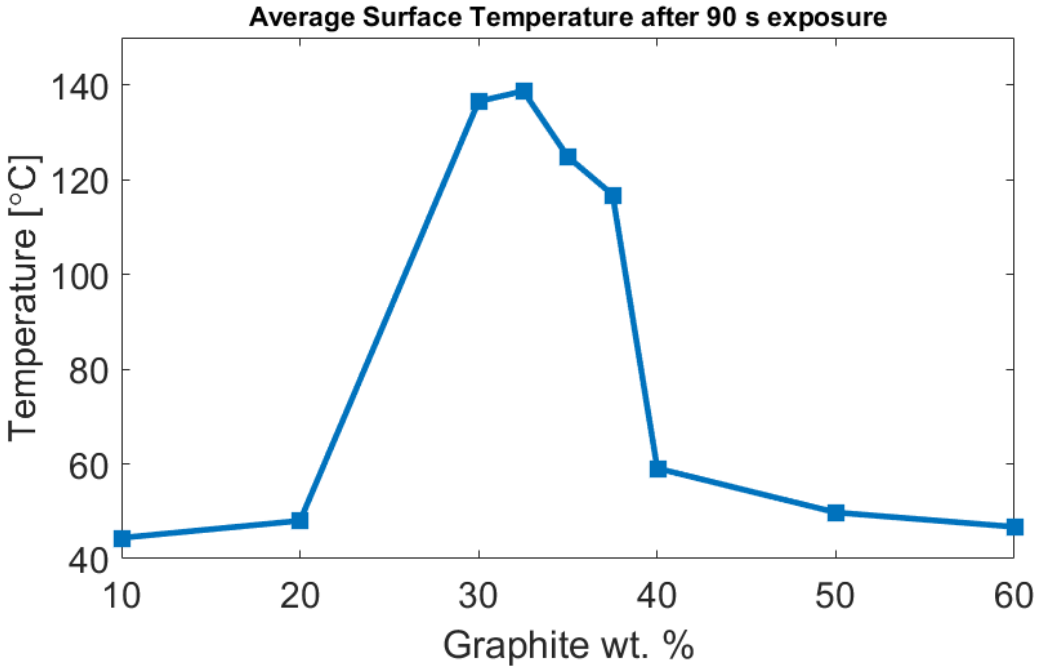

Figure 13 *Average surface temperature of the doped region after 90 seconds of RF exposure. The doped region was a circular cross section, and the tuning parameters of the RF generator were held constant.*

Very little heating occurred for graphite concentrations below 20% and above 40% by weight. However, the mixtures containing between 30% and 40% graphite produced a significant rise in surface temperature. The general trend from the RF heating experiments closely resembles the loss tangent data in Figure 11. The largest temperature rise occurred at approximately 32.5% graphite by weight, while the loss tangent was maximized at 35%. The limited heating in the lower concentrations can be attributed to the effective conductivity of the mixtures being sufficiently small to prevent substantial power loss. As the loading increased, the loss tangent reached a maximum, corresponding to a maximum heat generation in the RF experiments. At higher concentrations, however, the heating data and loss tangent data differ. The loss tangent gradually

declined after reaching a maximum, while the heating data showed a steep drop-off in temperature rise for concentrations above 40%. One possible explanation for the sharper decline in heating is the reduction in penetration depth that also occurred with increasing graphite content. At higher graphite concentrations, the combination of decreasing loss tangent and penetration depth caused a larger decline in heat generation than could be explained by the loss tangent alone.

In addition to the electrical properties, the geometry of the material has been shown to influence the heating characteristics in RF applications. The presence of sharp corners and flat faces can distort the electric field within the material and result in non-uniform heating (Uyar *et al.*, 2016)(Ferrari-John *et al.*, 2016). Considering the fusion of graphite-doped nylon mixtures, non-uniform heating is undesirable because it can lead to unintended geometric artifacts in the fused parts. To investigate the effect of geometry on heating, RF experiments were conducted using the circular, square, and rectangular forms to define different geometries. Thermal images of the powder surface provided an indication of heating uniformity by showing the temperature distributions across the powder bed. Previous heating experiments showed a maximum temperature rise at 32.5% graphite followed by a steep decline in heating as the concentration was increased. For this reason, a graphite loading of 30% by weight was chosen for the fusion experiments to compensate for the increased sensitivity in this region. In the absence of the conductive particles, the measured electrode voltage was approximately 1070 V_{rms}, corresponding to an estimated **E**-field strength of 170 V/cm. Figure 14 shows the surface temperature for a doped region with a circular cross section after five minutes of RF exposure. The electrodes in Figure 14 and subsequent infrared images were on the top and bottom with respect to the image, and the electric field direction is shown. The electrode voltage during the experiment was approximately

1,172 V_{rms}. Notably, the IR measurements demonstrated selective heating of the doped powder, while the surrounding virgin powder was nearly unaffected by the radiation.

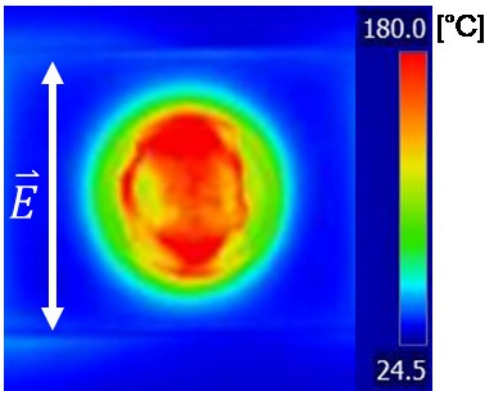

Figure 14 *Temperature profile after 5 minutes RF exposure for a doped region defined by a circular cross section. The electrodes are parallel to the top and bottom of the image, and the direction of the electric field is shown.*

The temperature profile of the circular cross section indicated a higher concentration of heat in the center with lower heating on the sides. Some of the irregularities on the surface were a result of the powder consolidating as it was heated beyond its melting point. As the powder densified, cooler surrounding powder fell from the sides and created what appeared to be cooler regions on the part surface.

The surface temperature distribution for a doped region with a square cross section is shown in Figure 15. The image was captured after six minutes of RF exposure, and electrode voltage was approximately 1,034 V_{rms}. The temperature pattern for the square geometry indicated highly non-uniform heating in which some regions were substantially hotter than their surroundings. In particular, thermal concentrations occurred at the corners and extended through the center of the part. Each of the flat edges of the square cross section were characterized by cooler regions near the center of the edge.

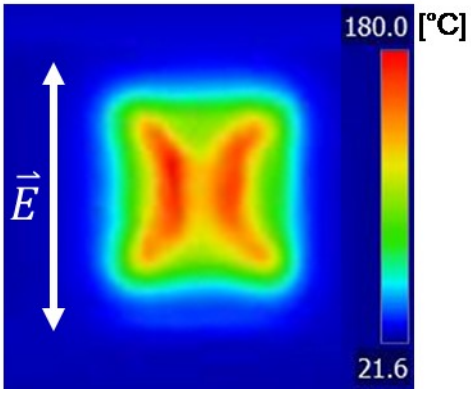

Figure 15 *Temperature profile after 6 minutes RF exposure for a doped region defined by a square cross section. The electrodes are parallel to the top and bottom of the image, and the direction of the electric field is shown.*

Figure 16 shows the temperature distribution after five minutes of RF exposure for a rectangular cross section. During the experiment, the electrode voltage was approximately 1,206 V_{rms}. Similar to the temperature pattern for the square cross section, the rectangular geometry showed highly non-uniform heating. Local hot spots in the corners of the rectangle were connected in the direction of the electric field, and the heating of the sides was substantially greater than in the center region. As with the circular cross section IR image, some of the irregularities were caused by the powder densification and subsequent powder falling to the molten surface.

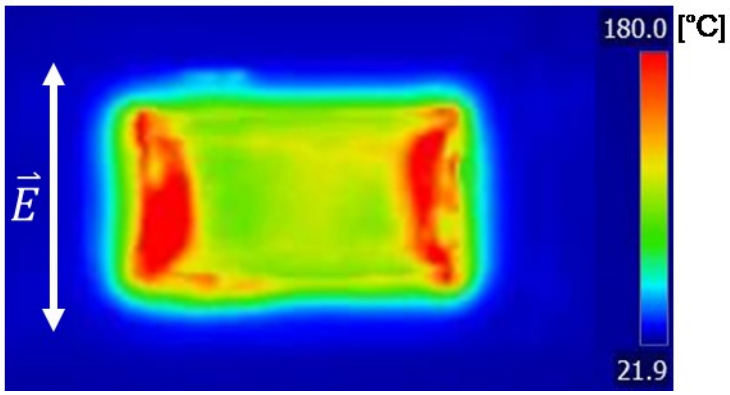

Figure 16 *Temperature profile after 5 minutes RF exposure for a doped region defined by a rectangular cross section. The electrodes are parallel to the top and bottom of the image, and the direction of the electric field is shown.*

RF radiation was applied to the samples until substantial portions of the surface exceeded the melting temperature of the nylon 12, which was approximately 180°C. In these regions, the

heat generation was sufficient to melt the nylon particles and allow fusion to take place before the powder bed cooled. As shown in Figures 17-19, the fused parts for each of the doped geometries highlighted the non-uniform heating that occurred as a result of the geometric definition. The total RF exposure time depended on the tuning parameters of the generator and the electrode voltage during the experiments. The heating times for the circular, square, and rectangular parts were five minutes, seven minutes and thirty seconds, and six minutes, respectively. In general, the shape of the parts matched the heating patterns in the IR images. However, out-of-plane curvature revealed effects that could not be predicted from the IR surface measurements. The circular cross section geometry produced a fused part that was elongated in the direction of the electric field with extreme curvature on the bottom surface. For the square cross section, the faces of the fused part were curved as the local cooler regions prevented fusion from taking place. The sides of the part were thicker in the direction of the electric field corresponding to the hotter regions in the thermal image of the powder surface. The fused geometry from the rectangular cross section followed trends similar to those found in the square, such that the faces were curved due to electric field distortions within the doped region. The side profile in Figure 19 highlights the thickening of the part on the sides in the direction of the electric field. Compared to the nominal dimensions of the doped geometries outlined in Section 2.4, the fused parts appeared to show shrinkage in all three coordinate axes. Two factors contributed to the part shrinkage with respect to the nominal dimensions. The nylon particles consolidated as the powder bed was heated above the melting temperature of the nylon, causing a reduction in the fused dimensions. Another source of the apparent shrinkage was insufficient heating in certain regions of the powder bed that prevented the particles from fusing.

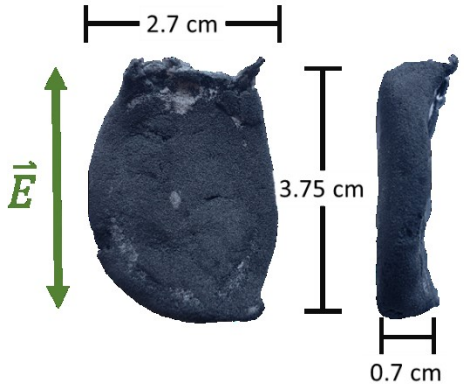

Figure 17 *Fused part created from a selectively doped powder bed in which the geometry was defined by a circular cross section. The doped region contained 30% graphite by weight, and the part was exposed to RF radiation for five minutes.*

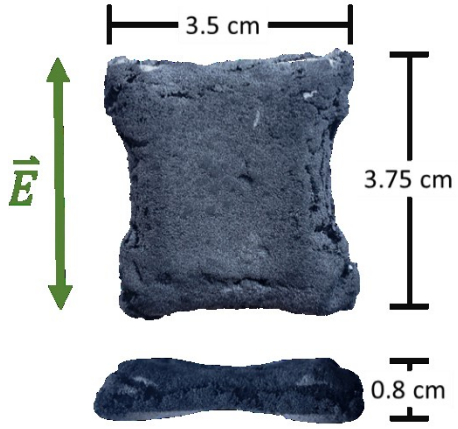

Figure 18 *Fused part created from a selectively doped powder bed in which the geometry was defined by a square cross section. The doped region contained 30% graphite by weight, and the part was exposed to RF radiation for seven minutes and thirty seconds.*

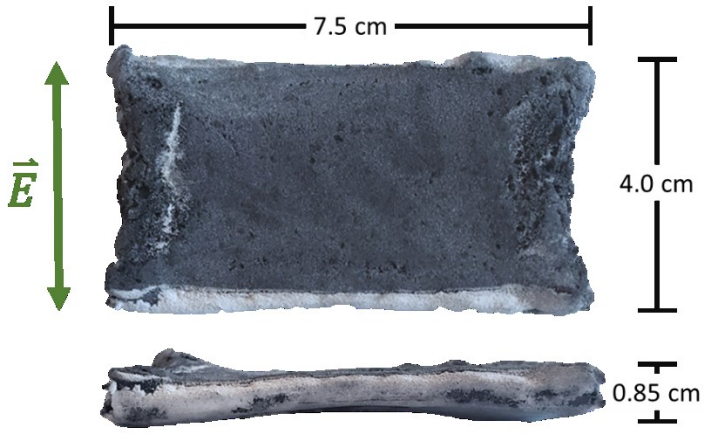

Figure 19 *Fused part created from a selectively doped powder bed in which the geometry was defined by a rectangular cross section. The doped region contained 30% graphite by weight, and the part was exposed to RF radiation for six minutes.*

Previous studies have investigated the geometric effect of heating uniformity in RF heating applications. Uyar et al. showed the development of temperature spikes at the edges and corners of block shaped foods subjected to RF radiation (Uyar *et al.*, 2016). Although the applied electric field in the doped nylon powder tests was approximately uniform, the field became distorted through interactions with the material. Non-uniform heating was caused by local field concentrations within the material. The geometric irregularities in the RF-fused nylon parts were similarly caused by electric field distortions. Future work seeks to improve the fused geometry by functionally grading the dopant throughout the powder bed to achieve more uniform heating within the parts.

Although the effects of geometry on heating uniformity require further investigation, the experiments demonstrated selective heating and volumetric powder fusion using RF radiation as the sole energy source. By combining particular proportions of nylon and graphite powders, the effective electrical properties of the composites were shown to generate sufficient heat from RF exposure to fuse the nylon particles.

3.3 Physical Properties of Fused parts

The degree of fusion and internal structure of the RF-fused parts were evaluated by machining the surfaces of the rectangular specimens to reveal an interior cross section. The faces were then inspected using an optical microscope as shown in **Figure 20**. The parts exhibited high levels of internal porosity with pores measuring as large as 1 mm in diameter. Porosity in laser sintered parts is often attributed to incomplete melting of the polymer particles and can result in the formation of voids within the parts (Bourell *et al.*, 2014). However, the spherical morphology of the voids in the machined specimens suggested the porosity was unlikely caused by incomplete particle melting. This is further corroborated by the lack of loose powder within the samples and

the absence of any partially sintered particles. Apart from the voids, the internal structure of the RF-fused samples appeared to show complete consolidation of the nylon particles. The voids within the parts were attributed to gas desorption from the graphite particles that trapped bubbles within the molten polymer. In experiments conducted by Hashiba et al., mixtures containing graphite powder showed a peak in CO_2 desorption at 200°C (Hashiba *et al.*, 1998). Similar temperatures were achieved during the RF heating experiments to ensure melting of the polymer, and thus gas desorption within the molten parts was possible.

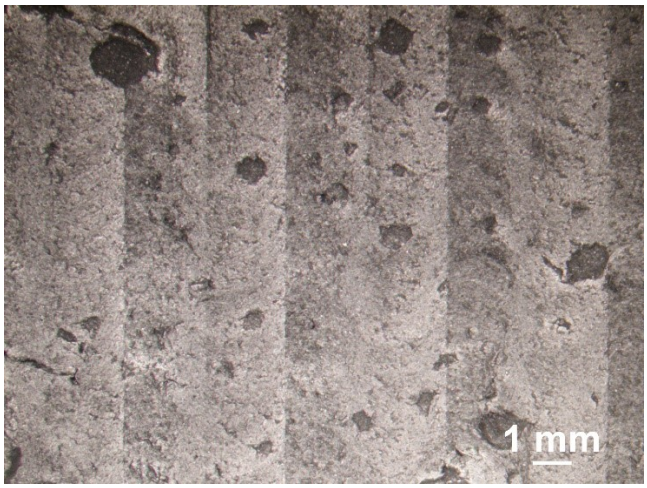

Figure 20 *Machined surface of RF-fused specimen showing the presence of large internal pores.*

The strength of the RF-sintered parts was evaluated by performing standard tension tests using an Instron (Norwood, MA, USA) model 3345 testing machine in a displacement-controlled experiment. The fused parts with a rectangular cross section were machined to conform with ASTM D638 type V standard tensile specimens. In total, five samples were created from the RF-sintered parts, and the mechanical properties were assessed. The specimens were tested according to ASTM D638 with a testing speed of 1 mm/min, and strain measurements were collected using an Epsilon Technology Corp. (Jackson, WY, USA) model 3442 extensometer.

The mechanical properties of the RF-sintered specimens were compared with the properties of laser sintered nylon 12 as reported by Starr et al. (2011), and the results are shown in Table 1. The error reported from the experimental results represents the standard error of the measurements across the five samples. In general, the mechanical properties of the RF-sintered parts were considerably poorer than laser sintered nylon 12, showing a reduction in the modulus, ultimate tensile strength, and elongation at break. The external and internal porosity on the samples likely contributed to the lower tensile strength and elongation by creating stress concentrations within the specimens. Examination of the fracture surfaces revealed the failure locations coincided with one of the voids in nearly every test, with a characteristic example depicted in Figure 21.

Table 1 *Mechanical properties of laser sintered nylon 12 compared with RF-sintered properties. The error from the experimental results corresponds to the standard error of the measurements across the five samples*

	Nylon 12 (Starr *et al.*, 2011)	Experiments
Tensile Modulus	1,760-1,870 [MPa]	1,361 ± 44 [MPa]
Ultimate Tensile Strength	11-55 [MPa]	16.5 ± 1.2 [MPa]
Elongation at Break	4-18 %	2.12 ± 0.35 %

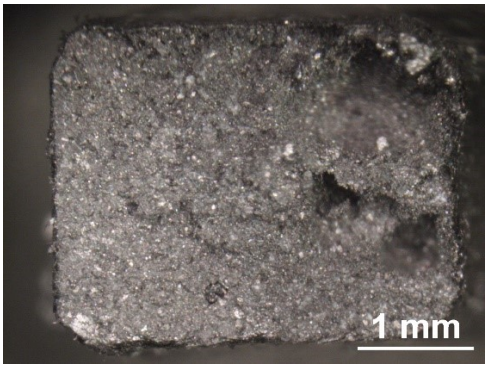

Figure 21 *Characteristic fracture surface from RF-fused samples showing large voids along the cross section.*

The reduction in mechanical properties of nylon 12 through the addition of graphite agrees with the results observed by Lee et al., where the introduction of carbon black and graphite

negatively impacted the flexural strength of the polymer composite (Lee *et al.*, 2009). The strength of the RF-fused parts could be improved by considering other forms of carbon for the dopant such as multi-walled carbon nanotubes. Previous studies have shown the addition of carbon nanotubes can also improve the electrical conductivity of the composites and reduce the amount of dopant necessary to achieve electrical percolation (Socher *et al.*, 2011). Further testing is required to improve the mechanical performance of RF-sintered parts and mitigate the formation of voids within them.

4. Conclusions

Composite mixtures of nylon 12 and graphite powder were shown to exhibit an insulator to conductor transition between graphite concentrations of 30% and 35% by weight. The effective electrical conductivity and relative permittivity increased with increasing graphite content, and the loss tangent reached a maximum at 35% graphite. Measurements of the surface temperature through RF heating experiments on the composite mixtures showed a similar trend to the loss tangent, such that the mixture with 32.5% graphite by weight generated the most heat. The doped powder mixtures were patterned into different geometries and surrounded by virgin powder to be used in additional RF heating tests. The samples were heated until the surface temperature in the doped region was above the melting temperature of the nylon, and fused parts were removed from the powder bed after cooling. The heating patterns from the IR images showed the presence of local hot and cold regions that were reflected in the fused parts as curvature along straight edges and thickening in the direction of the applied electric field. Towards the development of a volumetric AM process for thermoplastic polymers, efforts to mitigate the non-uniform heating for different geometries are required. However, the present work establishes the feasibility of a volumetric process where entire parts can be fused using RF radiation as the sole energy source,

thereby improving the processing speed over traditional AM techniques for thermoplastic polymers.

Future research initiatives seek to continue the development of a volumetric AM method for thermoplastic polymers by implementing a system capable of supplying the dopant to the powder bed in three dimensions. To that end, potential methods include depositing pre-mixed powders with a dosing mechanism or using an inkjet print head to selectively pattern the powder surface with an electrically conductive ink formulation. Novel approaches for improving the geometric accuracy of the sintered parts such as functional grading of the dopant are enabled by the selective patterning system. The functionally graded dopant distributions can be generated through computational design strategies and finite element analysis to improve heating uniformity. Modifying the alignment of the electrodes during heating is an alternative technique for improving the heating uniformity. Future work is aimed primarily at expanding the geometric complexity of sintered parts through process improvements and heating strategies.

Acknowledgements

This material is based on work supported by the National Science Foundation under Grant No. CMMI-1728015. Any opinions, findings, and conclusions or recommendations expressed in this material are those of the author and do not necessarily reflect the views of the National Science Foundation.

References

Ajoku, U., Saleh, N., Hopkinson, N., Hague, R. and Erasenthiran, P. (2006), "Investigating mechanical anisotropy and end-of-vector effect in laser-sintered nylon parts", *Proceedings of the Institution of Mechancial Engineers*, Vol. 220 No. 7, pp. 1077–1086.

Altemimi, A., Aziz, S.N., Al-Hilphy, A.R.S., Lakhssassi, N., Watson, D.G. and Ibrahim, S.A. (2019), "Critical review of radio-frequency (RF) heating applications in food processing", *Food Quality and Safety*, Vol. 3, pp. 81–91.

Arkema. (n.d.). "Thermoplastic Powders for Powder Bed Fusion", available at: https://www.arkema.com/en/markets-solutions/3d-printing/powder-bed-fusion/ (accessed 27 April 2020).

Asiabanpour, B., Khoshnevis, B. and Palmer, K. (2006), "Advancements in the selective inhibition sintering process development", *Virtual and Physical Prototyping*, Vol. 1 No. 1, pp. 43–52.

Bourell, D.L., Watt, T.J., Leigh, D.K. and Fulcher, B. (2014), "Performance limitations in polymer laser sintering", *Physics Procedia*, Vol. 56, pp. 147–156.

Cathcart, W.H. and Parker, J.J. (1946), "Defrosting frozen foods by high-frequency heat", *Journal of Food Science*, Vol. 11 No. 4, pp. 187–204.

Cathcart, W.H., Parker, J.J. and Beattie, H.G. (1947), "The treatment of packaged bread with high frequency heat", *Food Technology*, Vol. 1, pp. 174–177.

Cooke, W., Tomlinson, R.A., Burguete, R., Johns, D. and Vanard, G. (2011), "Anisotropy, homogeneity and ageing in an SLS polymer", *Rapid Prototyping Journal*, Vol. 17 No. 4, pp. 269–279.

Dahiya, H.S., Kishore, N. and Mehra, R.M. (2007), "Effect of percolation on electrical and dielectric properties of Acryllonitrile Butadiene Styrene/graphite composite", *Journal of Applied Polymer Science*, Vol. 106, pp. 2101–2110.

Deprez, N. and McLachlan, D.S. (1988), "The analysis of the electrical conductivity of graphite powders during compaction", *Journal of Physics D: Applied Physics*, Vol. 21, pp. 101–107.

Ferrari-John, R.S., Katrib, J., Palade, P., Batchelor, A.R., Dodds, C. and Kingman, S.W. (2016), "A tool for predicting heating uniformity in industrial radio frequency processing", *Food and Bioprocess Technology*, Vol. 9 No. 11.

Gibson, I. and Shi, D. (1997), "Material properties and fabrication parameters in selective laser sintering process", *Rapid Prototyping Journal*, Vol. 3 No. 4, pp. 129–136.

Gill, T.J. and Hon, K.K.B. (2004), "Experimental investigation into the selective laser sintering of silicon carbine polyamide composites", *Proceedings of the Institution of Mechancial Engineers*, Vol. 218 No. 10, pp. 1249–1256.

Goodridge, R.G., Tuck, C.J. and Hague, R.J.M. (2012), "Laser sintering of polyamides and other polymers", *Progress in Materials Science*, Vol. 57, pp. 229–267.

Hashiba, M., Hino, T., Shinbori, H., Deyama, S. and Chiyoda, H. (1998), "Gas desorption and adsorption properties of carbon based material used for cathode ray tube", *Thin Solid Films*, Vol. 332, pp. 141–145.

Haus, H. (1989), "Polarization", *Electromagnetic Fields and Energy*, Prentice-Hall, Englewood Cliffs, NJ, pp. 1–47.

Ho, H.C.., Cheung, W.L. and Gibson, I. (2002), "Effects of graphite powder on the laser sintering behaviour of polycarbonate", *Rapid Prototyping Journal*, Vol. 8 No. 4, pp. 233–242.

Hopkinson, N. and Erasenthiran, P. (2004), "High speed sintering-early research into a new rapid manufacturing process", *Solid Freeform Fabrication Symposium*, Austin, TX.

Jain, P.K., Pandey, P.M. and Rao, P.V.M. (2010), "Selective laser sintering of clay-reinforced polyamide", *Polymer Composites*, Vol. 31 No. 4, pp. 732–743.

Jansson, A. and Pejryd, L. (2016), "Characterisation of carbon fibre-reinforced polyamide manufactured by selective laser sintering", *Additive Manufacturing*, Vol. 9, pp. 7–13.

Kovacs, R. (1945), "High Frequency Currents and Apparatus", *Electrotherapy and Light Therapy*, pp. 187–204.

Lee, J.H., Jang, Y.K., Hong, C.E., Kim, N.H., Li, P. and Lee, H.K. (2009), "Effect of carbon fillers on properties of polymer composite bipolar plates of fuel cells", *Journal of Power Sources*, Vol. 193, pp. 523–529.

Manetsberger, K., Shen, J. and Muellers, J. (2001), "Compensation of non-linear shrinkage of polymer materials in selective laser sintering", *Solid Freeform Fabrication Symposium*, Austin, TX.

Marinković, S., Sužnjević, C. and Djordević, M. (1971), "Pressure dependence of the electrical resistivity of graphite powder and its mixtures", *Physica Status Solidi (A)*, Vol. 4, pp. 743–754.

Maxson, R. (1948), "Electrophysiotherapeutic apparatus".

Mehdizadeh, M. (2015), "Frequency allocations for industrial, scientific, and medical (ISM) applications", *Microwave/RF Applicators and Probes: For Material Heating, Sensing, and Plasma Generation*, William Andrew, Waltham, MA, pp. 369–370.

Metaxas, A.C. and Meredith, R.J. (1983), *Industrial Microwave Heating*, The Institution of Engineering and Technology, London, UK.

Michael, D., Mingos, P. and Baghurst, D.R. (1991), "Applications of microwave dielectric heating effects to synthetic problems in chemistry", *Chemical Society Reviews*, Vol. 20, pp. 1–47.

Negi, S., Dhiman, S. and Sharma, R.K. (2015), "Determining the effect of sintering conditions on mechanical properties of laser sintered glass filled polyamide parts using RSM", *Measurement*, Vol. 68, pp. 205–218.

Ohki, Y., Fuse, N. and Arai, T. (2010), "Band gap energies and localized states in several insulating polymers estimated by optical measurements", *2010 Annual Report Conference on Electrical Insulation and Dielectric Phenomena*, West Lafayette, IN.

Shen, J., Steinberger, J., Gopfert, J., Gerner, R., Daiber, F., Manetsberger, K. and Ferstl, S. (2000), "Inhomogeneous shrinkage of polymer materials in selective laser sintering", *Solid Freeform Fabrication Symposium*, Austin, TX.

Shusteff, M., Browar, A.E.., Kelly, B.E., Henriksson, J., Weisgraber, T.H., Panas, R.M., Fang, N.X., *et al.* (2017), "One-step volumetric additive manufacturing of complex polymer

structures", *Science Advances*, Vol. 3.

Socher, R., Krause, B., Hermasch, S., Wursche, R. and Potschke, P. (2011), "Electrical and thermal properties of polyamide 12 composites with hybrid fillers systems of multiwalled carbon nanotubes and carbon black", *Composites Science and Technology*, Vol. 71, pp. 1053–1059.

Starr, T.L., Gornet, T.J. and Usher, J.S. (2011), "The effect of process conditions on mechanical properties of laser-sintered nylon", *Rapid Prototyping Journal*, Vol. 17 No. 6, pp. 418–423.

Sun, J., Wang, W. and Yue, Q. (2016), "Review on microwave-matter interaction fundamentals and efficient microwave-associated heating strategies", *Materials*, Vol. 9, pp. 231–256.

Turk, D.-A., Brenni, F., Zogg, M. and Meboldt, M. (2017), "Mechanical characterization of 3D printed polymers for fiber reinforced polymers processing", *Materials and Design*, Vol. 118, pp. 256–265.

Uyar, R., Erdogdu, F., Sarghini, F. and Marra, F. (2016), "Computer simulation of radio-frequency heating applied to block-shaped foods: Analysis on the role of geometric parameters", *Food and Bioproducts Processing*, Vol. 98, pp. 310–319.

Wang, X., Li, Z., Chen, Z., Zeng, L. and Sun, L. (2018), "Structural modification of carbon black for improving the dielectric performance of epoxy based composites", *Advanced Industrial and Engineering Polymer Research*, Vol. 1, pp. 111–117.

Xu, Z., Wang, Y., Wu, D., Ananth, K.P. and Bai, J. (2019), "The process and performance comparison of polyamide 12 manufactured by multi jet fusion and selective laser sintering", *Journal of Manufacturing Processes*, Vol. 47, pp. 419–426.

Yacubowicz, J. and Narkis, M. (1986), "Dielectric behavior of carbon black filled polymer composites", *Polymer Engineering and Science*, Vol. 26 No. 22, pp. 1568–1573.

Zhang, W., Blackburn, R.S. and Dehghani-Sanij, A.A. (2007), "Effect of carbon black concentration on electrical conductivity of epoxy resin-carbon black-silica nanocomposites", *Journal of Materials Science*, Vol. 42, pp. 7861–7865.

Zhou, W., Chen, Q., Sui, X., Dong, L. and Wang, Z. (2015), "Enhanced thermal conductivity and dielectric properties of Al/β-SiCw/PVDF composites", *Composites: Part A*, Vol. 71, pp. 184–191.

Zhou, W., Gong, Y., Tu, L., Xu, L., Zhao, W., Cai, J., Zhang, Y., *et al.* (2017), "Dielectric properties and thermal conductivity of core-shell structured Ni@NiO/poly(vinylidene fluoride) composites", *Journal of Alloys and Compounds*, Vol. 693, pp. 1–8.